Journal of Materials Chemistry C

Evolutionary Structure Prediction of Two-dimensional IrB_{14}: A Promising Gas Sensor Material

Journal:	*Journal of Materials Chemistry C*
Manuscript ID	TC-ART-03-2018-001354.R1
Article Type:	Paper
Date Submitted by the Author:	23-Apr-2018
Complete List of Authors:	YU, JUN; National Institute of Advanced Industrial Science and Technology Tsukuba Center Tsukuba Central Khazaei, Mohammad; RIKEN Advanced Institute for Computational Science, Computational Materials Science Team Umezawa, Naoto; National Institute for Materials Science (NIMS), International Center for Materials Nanoarchitectonics (MANA) Wang, Junjie; Tokyo Institute of Technology, Materials Research Center for Element Strategy

Journal of Materials Chemistry C

ARTICLE

Evolutionary Structure Prediction of Two-dimensional IrB_{14}: A Promising Gas Sensor Material

Received 00th January 20xx,
Accepted 00th January 20xx

DOI: 10.1039/x0xx00000x

www.rsc.org/

Jun Yu[#, a], Mohammad Khazaei[#, b], Naoto Umezawa[b, c], Junjie Wang[*, b, d]

Two-dimensional (2D) boron structures, in which boron atoms arrange in a 2D manner, have attracted broad attention for their potential applications in nanoelectronic devices. To improve the stability of 2D boron and find new functionalities, we predict a series of sandwich-shaped 2D structures of IrB_x ($8 \le x \le 16$) through employing *ab initio* evolutionary structure search. It is demonstrated that the stability of 2D boron sheet is greatly improved with the introduction of Ir atom. Among various compositions, it turns out that 2D IrB_{14} is thermodynamically more stable than the mixture of the known IrB_9 compound and α-boron. Moreover, we have studied the gas sensitivity of the 2D-IrB_{14} to the adsorption of CO and CO_2 molecules. It is found that CO gas molecules bind chemically to the boron atoms, whereas CO_2 molecules do not. Upon CO adsorption, there is a charge transfer from surface atoms to CO molecule. Hence, acceptor states are formed above the Fermi energy indicating that IrB_{14} is a promising novel 2D gas sensor material.

Introduction

Recently, motivated by theoretical predictions on stability of 2D boron sheets,[1-12] several research groups have synthesized monolayers of boron phases on silver or copper surfaces,[13-15] indicating borophene as a new member of the growing family of two-dimensional materials. Besides the study on the pure boron phases, there exists an extensive interest on the 2D metal borides, which are a big family of ceramic materials with superior mechanical and electronic properties. For examples, Zhang et al.[16] have predicted several FeB_6 monolayer structures[17] and revealed the semiconducting properties in contrast to the metal/semimetal feature of 2D boron. Shortly thereafter, Xu et al.[18] obtained several sandwich-shaped structures of FeB_6 by using USPEX code[19-21] that are more stable than those monolayers predicted previously while also possessing semiconducting properties. Though these studies provided interesting insight into the possible structures of 2D borides, feasibility of synthesizing the predicted structures has not been considered. This can be evaluated by comparing the stability of existing phases (e.g. Fe and FeB_2 bulk) with the predicted compound (e.g. FeB_x nanosheet). To address this drawback, Wang et al.[22] have carried out a systematic study for the Ti-B system. Using the *ab initio* evolutionary structure search algorithm USPEX, they have predicted a series of TiB_x ($2 \le x \le 16$) structures and estimated their globally thermodynamic stabilities with respect to the known materials of Ti metal, α-boron sheet and bulk TiB_2. Among those predicted structures, the formation energy of TiB_{12} was found to be comparable with that of a mixture of the well-known TiB_2 compound and a 2D α-boron sheet. A quasi-Dirac point with a 0.02 eV gap and tunable electronic properties (work function and conductivity) by strain were observed for this predicted 2D TiB_{12}.

Considering the abundance of metal borides, these studies have dramatically expanded the diversity and application perspective of 2D boron. Many planar hyper-coordinated $TM@B_n$ (n=7-10) structures[23-25] with neutral or charged states have been examined theoretically and experimentally, where TM is a transition metal, e.g. Fe, Co, Ir, and etc. These planar hypervalent boron motifs can probably be used to synthesize novel 2D-TMB_x in the future. However, the possibility of realizing 2D-TMB_x is still doubtful due to the presence of competing phases such as highly stable bulk boride that are potentially formed during the synthesis process. Therefore, the most ideal condition of avoiding this competition is to design a 2D-TMB_x structure by choosing a combination of TM and boron that the corresponding boride bulk does not exist.

In the present work, we have carried out a systematic structure search for the 2D IrB_x (x=8, 10, 12, 14 and 16) system by employing *ab initio* evolutionary algorithm implemented in USPEX. The reason why we have chosen to study the 2D IrB_x is that the planar hypervalent IrB_9 ring has recently been synthesized[25] and shows promise as precursor of synthesizing 2D IrB_x. Because we propose that the 2D IrB_x would be

[a] Advanced Manufacturing Research Institute, National Institute of Advanced Industrial Science and Technology, 1-2-1 Namiki, Tsukuba, Ibaraki, Japan.
[b] International Center for Materials Nanoarchitectonics (MANA), National Institute for Materials Science, 1-1 Namiki, Tsukuba, Ibaraki 305-0044, Japan.
[c] Samsung Electronics, Semiconductor R&D Center, 1, Samsungjeonja-ro, Hwaseong-si, Gyeonggi-do 18448, Korea
[d] Materials Research Center for Element Strategy, Tokyo Institute of Technology, 4259 Nagatsuta-cho, Midori-ku, Yokohama, Kanagawa 226-8503, Japan.
[#] These authors contributed equally.
[*] wang.junjie0810@gmail.com
Electronic Supplementary Information (ESI) available. See:
DOI: 10.1039/x0xx00000x

synthesized through the reaction of IrB_9 and boron, the compositions with low B content, such as IrB_2, IrB_4 and IrB_6, were not considered in present study. The predicted structures for these compositions are found to be sandwich-shaped as expected and show improved stability compared with 2D boron. In particular, the predicted most stable 2D-IrB_{14} structure exhibits even higher stability than other known competing phases such as bulk Ir, IrB_9 molecule, α-boron sheet and bulk. Moreover, there is no known stable compounds as competing phases in Ir-B system, except two reported alloy phases with ambiguous compositions of $IrB_{1.1}$ or $IrB_{1.35}$.[26, 27] Therefore, the experimental synthesis of this 2D-IrB_{14} is highly expected. Furthermore, our investigations on of stabilities and electronic structures of CO and CO_2 molecules on the 2D-IrB_{14} indicate that CO molecule is chemically bound on the surface with significant adsorption energy, while CO_2 adsorption is very unlikely. It was found that the adsorption of CO on 2D-IrB_{14} gives rise to acceptor states above the Fermi energy, which induce charge transfer from 2D nanosheet to CO. This finding leads to the idea that the predicted 2D-IrB_{14} can be used as a novel CO gas sensor material.

Computational Methods

Our calculations were done in three steps: In the first step, *ab initio* evolutionary structure searches were carried out using the Universal Structure Predictor: Evolutionary Xtallography (USPEX) and VASP codes.[19-21, 28, 29] With defined Ir/B ratio, number of atoms per cell and initial thickness of the 2D structures, USPEX produced many 2D-IrB_x structures as the first generation which are produced by a random-number generator. The global optimization for the most stable crystal structure was conducted through iterative procedure of evolutionary variation operations of USPEX until the lowest-energy structure remained unchanged for a sufficiently large number of generations. The local optimization, i.e. structure relaxation and total energy calculations were performed by VASP for all the candidate structures in each generation. A size constraint of less than 40 atoms per cell was applied on the slab models during the 2D structure search. Details regarding the evolutionary structure search can be referred in the literature.[19-22, 30, 31] To efficiently optimize the thousands of structures produced by USPEX, sufficient settings were used: the energy cutoff for the plane-wave basis set expansion was set at 400 eV, and the Monkhorst–Pack k-point mesh solution in reciprocal space was $2\pi \times 0.06$ Å^{-1} for all structures. We adopted generalized-gradient approximation (GGA) in the Perdew–Burke–Ernzerhof revised for solids (PBEsol)[32] form to describe the exchange correlation interaction in all calculations of present work.

In the second step, the most stable structures, which are obtained in the evolutionary structure searches, were re-optimized with high precision setting: cutoff energy of 600 eV and k-point sets of $2\pi \times 0.02$ Å^{-1} (convergence test of k-mesh is shown in Figure S1). The thermodynamic stabilities of the optimized structures were examined relative to the available competing phases of bulk Ir, planar IrB_9 molecule, α-boron sheet and bulk. Furthermore, the dynamic stability of most stable structure IrB_{14} was confirmed by phonon dispersion calculation performed using the linear response method[33] implemented in CASTEP.[34] Finally, the thermal stability of the predicted 2D-IrB_{14} structure was checked by performing a set of long time first-principles molecular dynamics (FPMD) simulations using canonical ensemble (NVT). A vacuum thickness of 30 Å along Z direction was adopted to avoid interaction between the 2D structure with its images.

In the final step, the adsorptions of CO and CO_2 molecules on the surface of 2D IrB_{14} were investigated through performing FPMD and quasi-static structure optimization. In these simulations, a slab model of 2D-IrB_{14} structure with 2 × 2 supercell (4 Ti atoms and 56 B atoms) was adopted. To keep the symmetry of 2D model, CO molecule was introduced on either side of the slab. The time step of 3fs and temperature of 298 K were set in the FPMD and the atomic coordinates of total 1500 steps were collected. The adsorption energies of CO and CO_2 molecules $E_{ad}(X)$ (X indicates CO or CO_2) on the surface of 2D-IrB_{14} were calculated using following equation:

$$E_{ad}(X) = E_{tot}(X/IrB_{14}) - E_{tot}(X) - E_{tot}(IrB_{14}) \quad (1)$$

where $E_{tot}(X/IrB_{14})$ is the total energy of optimized configuration of 2D-IrB_{14} with adsorbed CO or CO_2 on it, and $E_{tot}(IrB_{14})$ is the total energy of surface model.

The charge transfer between 2D-IrB_{14} and adsorbed CO was studied by performing charge density difference calculations defined as:

$$\rho_{diff} = \rho(CO/IrB_{14}) - \rho(CO) - \rho(IrB_{14}) \quad (2)$$

where $\rho(CO/IrB_{14})$, $\rho(CO)$, and $\rho(IrB_{14})$ are the charge densities for CO/IrB_{14}, CO and IrB_{14} systems, respectively. The charge densities of the latter two systems are obtained based on a set of single point total energy calculations for the separated CO or IrB_{14} system by using their coordinates in CO/IrB_{14}.

The infrared vibrational frequency of the free CO molecule and the CO molecule on IrB_{14} was computed in terms of the oscillator strengths determined by the Born effective charges and the displacement vectors[35]:

$$I(\omega) = \sum_{\alpha=1}^{3} \left| \sum_{l=1}^{M} \sum_{\beta=1}^{3} Z^*_{\alpha\beta}(l) e_\beta(l) \right|^2 \quad (3)$$

where $e_\beta(l)$ is the normalized vibrational eigenvector of the ω^{th} mode, α and β indicate the Cartesian polarizations, l labels the different atoms of the system, and $Z^*_{\alpha\beta}(l)$ is the Born effective charge tensor of the l^{th} atom of the calculated system.

Results and Discussion

Figure 1 shows the geometrical structures of the most stable configurations for IrB_8, IrB_{10}, IrB_{12}, IrB_{14} and IrB_{16}, which have been obtained through our extensive structure searches. All of them are "sandwich"-shaped structures with mirror symmetries with the Ir atoms at the mid layer. At first, we investigated the thermodynamic stabilities of the predicted structures by calculating formation energies relative to the bulk iridium and α-boron sheet: $E_f = (E_{IrBx} - E_{Ir} - x \cdot E_B)/(x+1)$. E_{IrBx}, E_{Ir} and E_B are respectively the energy of one formula unit of 2D IrB_x, energy per atom in bulk iridium and α-boron sheet. The data shown in Fig. 1 imply that all 2D-IrB_x are thermodynamically more stable than the physical mixture of

iridium bulk and α-boron sheet. However, only the 2D-IrB_{14} (Cmmm) is both globally and thermodynamically stable because its formation energy lies on the convex hull (Fig. 1). We have also checked the stability of 2D-IrB_{14} with respect to previously predicted 2D boron sheets, available IrB_9 hyper-coordinated structure, as well as α-boron bulk. Table 1 shows that the formation energies of IrB_{14} relative to iridium bulk and other reported boron sheets are all negative. Moreover, the formation energy of IrB_{14} with respect to IrB_9 and α-boron bulk is -0.57 eV/atom. This means that IrB_9 and α-boron bulk can be used as precursors to synthesize 2D-IrB_{14} by chemical/physical vapor deposition. And the synthesized 2D-IrB_{14} will not decompose into 2D boron and Ir bulk.

The stabilities of all predicted structures were also checked by a set of phonon-dispersion calculations (Supporting Information Figure S2). 2D-IrB_{14} is proved to be dynamically stable because no imaginary frequency is observed in its phonon band structure (Figure S2 (a)). In addition, all phonon modes for IrB_{12} and IrB_{16} are also positive (Figures S2 (d) and (e)), which indicates that though these systems are metastable according to the formation energy calculations, it might be possible to synthesize them in a particular experimental condition. Meanwhile, IrB_8 and IrB_{10} are unstable due to the appearance of imaginary frequencies around Γ point (Figures S2 (b) and (c)).

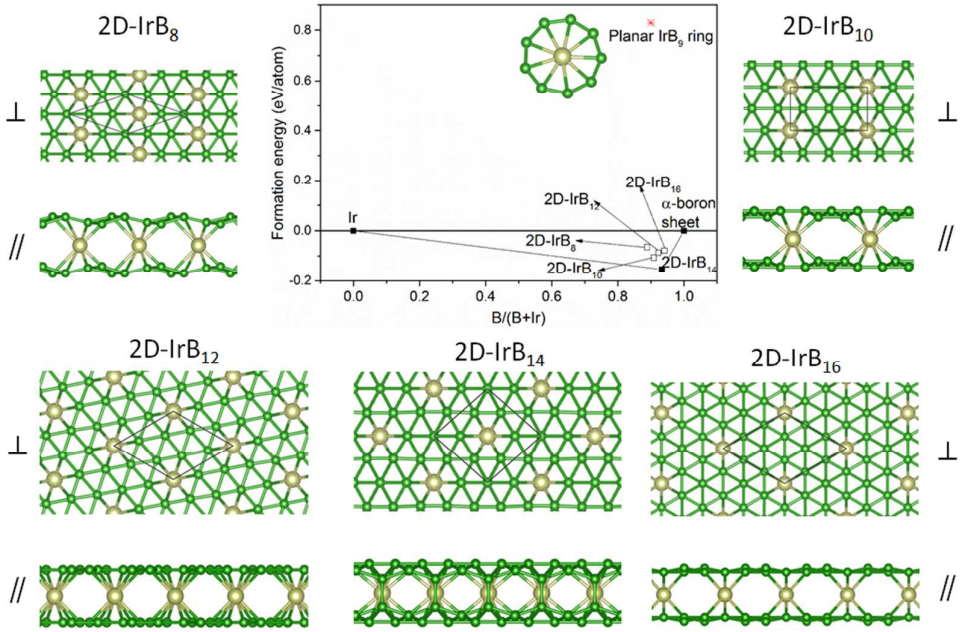

Figure 1 The results of an evolutionary structure search for 2D-IrB_x system: computed formation energies per atom and crystal structures of predicted 2D-IrB_x (x=8, 10, 12, 14 and 16). The solid filled square symbols indicate the stable structures of Ir-B system, whereas empty squares indicate the possible metastable phases. The formation energy of planar IrB_9 ring, which was synthesized in experiment,[25] is presented (red star) as a reference. The gold and green balls represent Ir and B atoms, respectively. The symbols of ⊥ and // respectively indicate the top and side views of the predicted 2D-IrB_x structures.

Table 1 The computed formation energies of IrB_{14} relative to different reference phases.

Reference phases	Ir bulk + α-boron sheet	Ir bulk + reported most stable boron sheet[5]	IrB_9 + α-boron bulk
Formation energy (eV/atom)	-0.15	-0.07	-0.57

The electronic structures of the predicted 2D-IrB_{14} were calculated and are shown in Figs. 2 and 3. To understand the role of Ir atom in the stabilization of 2D boron, the electronic structures of pure 2D-B_{14} structure, in which Ir atoms are removed from the 2D-IrB_{14} structure leaving the positions of boron atoms unchanged, is also shown in Figs. 2 and 3 for comparison. As shown in Fig. 2 (a), the calculated ELF with an isosurface of 0.7 highlights the coexistence of covalent 2c–2e (two-centre two-electron) and multicenter–2e (multicentre two-electron) bonds among the B atoms. Interestingly, electron accumulation is observed (Figs. 2(a)) between Ir and B atoms and the plotted ELF map along the co-plane of Ir and B atoms clearly shows an ELF maximum (Fig. 2(b)), suggestive of covalency of bonding. It is seen that in IrB_{14}, the Ir-B bonds

have covalent nature, which is in contrast to ionic nature of Ti-B and Fe-B bonds in 2D-TiB_{12} and 2D-FeB_6. The above difference is originated from the different electroegativities of the transition metals: Ti(1.54), Fe(1.83) and Ir(2.20). Since the electronegativities of Ti and Fe are much lower than that of B (2.04), a significant charge transfer occurs from Ti or Fe to B atoms resulting in typical ionic bonding Ti-B and Fe-B in 2D-TiB_{12} and 2D-FeB_6. Ir and B atoms possess comparable electronegativities of 2.20 and 2.04, which does not allow for a large charge transfer and results in a covalent bond. 2D-boron structure can be regarded as an electron-deficient system (Figs. 2 (c) and (d)). An electron-deficient region can be observed at the center of the B_{14} structure without Ir atom (Fig. 2(d)). The calculated difference in the charge density between the structures with and without Ir atom in IrB_{14} exhibits that charge transfer and charge redistribution occurs between Ir and neighboring B atoms (Fig. 2(e)).

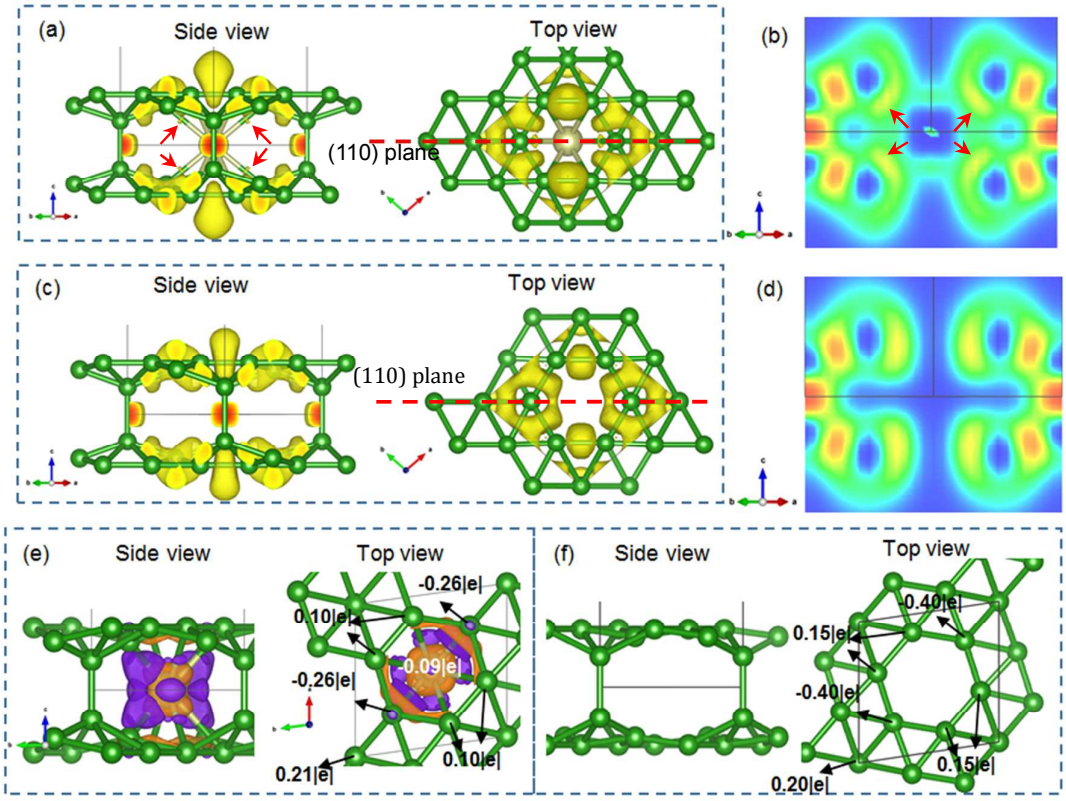

Figure 2 Electronic structures of 2D-IrB_{14} and B_{14} (obtained by removing Ir atom from IrB_{14} structure): isosurfaces of electron localization function (ELF) plotted with the value of 0.7 ((a) and (c)) and ELF maps along (110) surfaces ((b) and (d)) for 2D-IrB_{14} ((a) and (b)) and 2D-B_{14} ((c) and (d)), and the calculated Bader charges of 2D-IrB_{14} (e) and 2D-B_{14} (f). The red arrows in (a) and (b) indicate the position of electron accumulation between Ir and B atoms. The positions of (110) planes for (b) and (d) are indicated using red dash lines in (a) and (c). The charge density difference with and without Ir atom is also shown in (e) to indicate the charge transfer between Ir and B atoms.

Bader charge analysis (indicated in Fig. 2(e)) confirms that only a very small amount of charge (0.09 |e|) was transferred from B atoms to Ir atom. This observation is in contrast to the charge transfer phenomena observed in the previous studies on TiB_{12} and FeB_6. In the previous work, it was seen that the significant charge transfer occurs from Ti to B in TiB_{12} (1.33 |e|)[22] and from Fe to B in FeB_6 (0.192 |e|)[18], which was regarded as the main reason for the improved stabilities of 2D-TMB_x structures. This is because by receiving additional electrons from transition metal atoms, the B-B bonds get stronger. However, our study reveals here that the charge transfer from transition metal to B atoms is unlikely to be the critical mechanism for the stabilization of boron sheet in 2D-IrB_{14}. Instead, we suggest that the formation of covalent bonding between transition Ir and B atoms could dominantly stabilize the boron sheet.

The computed electronic band structure (Fig. 3 (a)) shows that 2D-IrB_{14} is metallic, which is different from the semi-metallic TiB_{12}[22] and semiconducting FeB_6[16, 18] predicted in previous studies. Pure 2D-B_{14} is a semimetal with a pseudo-gap at Fermi level (Fig. 3(b)). The projected density of states (Fig. 3(d)) shows that B(s+p_{xy}) and B(p_z) are respectively dominant in valence band and conduction band. This reveals that the in-plane sigma bonds are the main reason for the stability of 2D-B_{14}. As shown in Fig. 3(c), upon introduction of Ir atom into 2D boron, electrons are transferred from B(s+p_{xy}) to B(p_z) state.

The conduction bands of 2D-B_{14} are mainly composed of B states while the valence bands result from the hybridization of B and Ir(d) states. The strong resonance between B(sp) and Ir(*d*) states (Fig. 3(c)), which reveals formation of bonds between Ir and B atoms, can be observed in energy range of -3.5 eV ~-2 eV of Fig. 3(c). This indicates that electrons of boron atoms were re-distributed in a way to form in plane Ir(d_{xy})-B(s+p_{xy}) and out of plane Ir(d_z^2)-B(p_z) covalent bonds. This rearrangement of electrons dramatically enhances stability of the 2D structure.

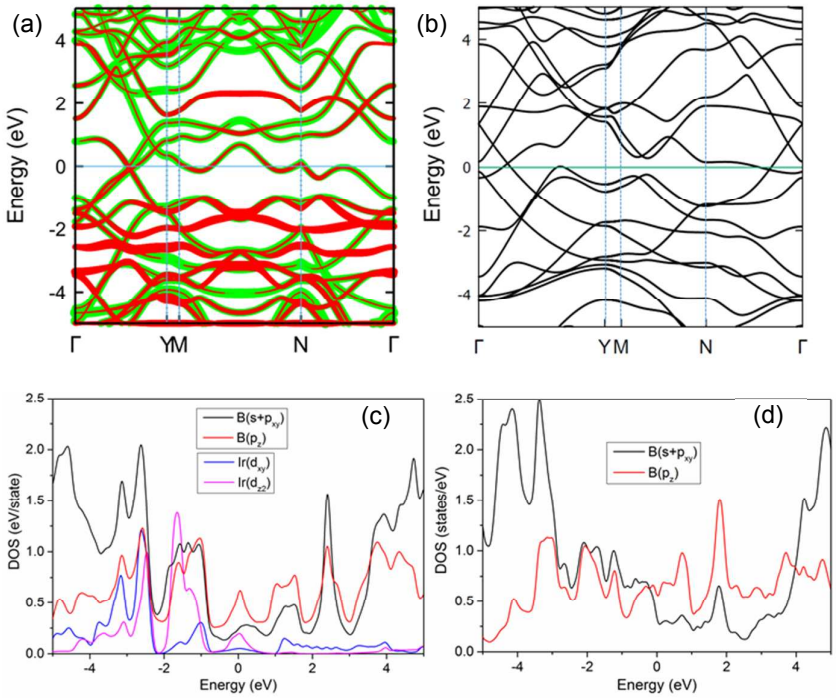

Figure 3 Calculated band structures ((a) and (b)) and decomposed densities of states ((c) and (d)) for 2D-IrB_{14} ((a) and (c)) and B_{14} ((b) and (d)). Green and red dots in the projected band structure indicate the contributions of boron and titanium atoms, respectively.

Due to the high carrier mobility and the high sensitivity to adsorbates, graphene and carbon nanotubes have been considered as promising materials for sensor applications.[36-40] The 2D-IrB_{14} structure predicted in this study, in addition to its improved stability relative to boron sheets, exhibits excellent metallic feature similar to the 2D boron with high carrier mobility [5, 10]. Therefore, the interaction of toxic gases with the 2D-IrB_{14} is an interesting topic that is worth be investigated. In present work, the adsorptions of CO and CO_2 molecules on the 2D-IrB_{14} were studied using first-principles molecular dynamics (FPMD), quasi-static structure optimization and electronic structure calculations. In the present study, a 1/7 monolayer (ML) coverage of CO/CO_2 was considered.

At first, we investigated the possible adsorption configurations of CO and CO_2 molecules on 2D-IrB_{14} using FPMD and quasi-static structure optimization. The CO and CO_2 molecules were initially placed 2.5 Å above the 2D-IrB_{14} surface, with the C-O axis vertical to the surface over different sites. FPMD simulations of 4500 fs at 298 K show that CO molecule is quickly adsorbed on the 2D-IrB_{14} after about 500 fs (Fig. 4 (a)), whereas CO_2 molecule exhibits an oscillatory movement (Fig. 4 (b)) between the two surfaces of 2D-IrB_{14}: firstly moves away from one surface where it was initially put and approaches to the second surface of 2D-IrB_{14} sheet across the vacuum layer; then moves back when the distance to the second 2D-IrB_{14} surface is about 3 Å. Figure 4 (c) shows the local geometry near CO molecules are adsorbed on the 2D-IrB_{14} surface chemically with a B-C bond distance of about 1.5 Å, which is much shorter than the bond distance of physically adsorbed CO on the graphene (2.9 Å).[39] This indicates that the adsorption of CO on 2D-IrB_{14} is stronger than that on graphene.[37] The result of FPMD simulations is further supported by the structure relaxations. It shows a consistent result with the FPMD simulation that the most stable CO adsorption configuration on 2D-IrB_{14} locates on top of a B atom (Fig. 4 (d)). The optimized C-B distance is 1.503 Å, which is very close to the result of FPMD simulation. The calculated CO adsorption energy for this most stable configuration is -0.45 eV, which indicates a much stronger adsorption than that the reported for CO adsorption on graphene, -0.12 eV.[39] Similar to the FPMD results, no stable CO_2 adsorption configuration can be observed through the quasi-static structure relaxations, which reveals that the adsorption of CO_2 molecule on 2D-IrB_{14} is energetically unfavorable. To combine the result of FPMD simulation and structure relaxation, we can suggest that CO can be selectively adsorbed on 2D-IrB_{14} surface from the mixture of CO and CO_2. To study the CO adsorption behavior at high temperature condition, the final

CO adsorption configuration of FPMD simulation at 298K was further annealed at 500, 1000, 1500, and 2000 K for 4500 fs. As shown in Figure S3, 2D IrB_{14} shows no sign of disruption even at 2000 K. It is observed that the CO molecules can be adsorbed on the 2D IrB_{14} surface at the temperatures as high as 1000K. CO molecules start being desorbed from the 2D IrB_{14} surfaces when the simulation temperature reaches to 1500 K. This series of FPMD simulations reveal that 2D-IrB_{14} can efficiently adsorb CO in a wide temperature range from room temperatures to an elevated temperature, e.g., 1000K, and the adsorbed CO molecules can be desorbed by simply heating the material to higher temperatures. It indicates the potential application of 2D-IrB_{14} as a gas sensor material to detect CO from a mixture of CO and CO_2.

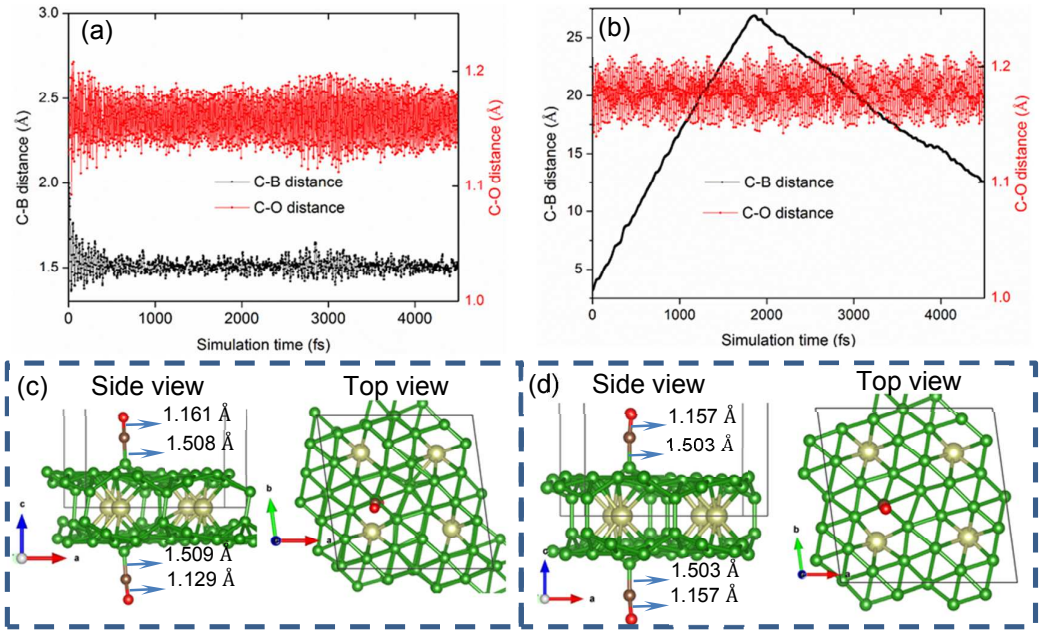

Figure 4 FPMD simulation results of (a) CO and (b) CO_2 on the 2D-IrB_{14} surfaces at 298K, (c) the final configuration of CO adsorption on 2D-IrB_{14} surfaces by FPMD at 298K, and (d) the most stable CO adsorption configuration on 2D-IrB_{14} surfaces optimized with density functional theory calculations. In the FPMD simulations presented in this figure, the CO and CO_2 were vertically placed 2.5 Å above the B atom of 2D-IrB_{14}. The time evolutions of C-O bond length and the distance between C atom and B atom at one surface of 2D-IrB_{14} are shown in (a) and (b).

Considering the above observation that only CO molecule can be adsorbed on the 2D-IrB_{14} surface, we have carried out electronic structure calculations for the CO adsorbed configuration only. The electronic band structure (Figure 5 (a)) shows that the CO adsorbed 2D-IrB_{14} has a stronger metallic feature comparing with the pristine 2D-IrB_{14}. When the CO molecule is adsorbed, two unoccupied CO-related states appear above the Fermi energy, which are indicated as {c} region in Fig. 5 (a). The states located in {d} region indicate the highest occupied states (Fig. 5 (a)). The calculated density of states (DOS) in Figure 5(b) show a strong resonance between the *p* orbitals of CO molecule and *p* and *d* orbitals of B and Ir atoms in the energy range -8.5 eV to -7.5 eV (bonding) and {c} from 0.5 eV to 3.5 eV (antibonding). Region {d} also receives dominant contribution from the IrB_{14} orbitals hybridized with CO atomic orbitals.

The partial charge densities corresponding to bands in {c} and {d} regions in Fig. 5 (a) are plotted in Fig. 5 (c) and (d), respectively. One can see that these unoccupied states are strongly mixed with the molecular orbitals of CO molecule and act as acceptor states. Therefore, the CO adsorbed 2D-IrB_{14} is expected to have an altered conductivity property. The spatial distribution of the total charge density difference before and after the CO adsorption is shown in Fig. 5(e). The adsorption of the CO molecule clearly gives rise to the charge transfers between the C atom in the CO molecule and the B atom in the 2D-IrB_{14} due to the hybridizations between their *p* orbitals as discussed above. Bader charge analysis shows that about 0.48 |e| is moved from 2D-IrB_{14} to per CO molecule during the adsorption process. It is noteworthy that the charge transfer in the present study corresponds to a CO coverage of one molecule per four IrB_{14} formulas. This significant amount of charge transfer leads to the dramatic change in the electronic structure from metal to semimetal. It is noteworthy that SnO_2 has already been proposed as being a gas sensor materials for CO toxic gas because of the charge transfer from the C atom in the CO molecule to SnO_2 surface (around 0.26 |e|).[41] This is much lower than the charge transfer between CO and 2D-IrB_{14}. Moreover, 2D-IrB_{14} can avoid the main drawback of SnO_2 sensor materials that the surface can become less sensitive due to reaction of CO with surface O atoms to form CO_2.

In addition, the infrared (IR) spectra of CO molecule on 2D-IrB_{14} and free CO molecule were calculated to exhibit the influence of the charge transfer from 2D-IrB_{14} to CO on vibration frequency of CO (shown in Figure S4). Our calculations show a redshift of about 2 cm^{-1} of the vibrational frequency of CO molecule absorbed on 2D-IrB_{14} (2119.5 cm^{-1}) in comparison with that of free CO molecule (2121.3 cm^{-1}), which is due to the charge transfer from 2D-IrB_{14} to the antibonding orbitals of CO weakens the carbon-oxygen bond. The result is consistent with that observed for CO adsorption on reduced TiO_2 surface.[42]

Moreover, as shown in Figs. 5 (f) and (g), the pristine and CO-adsorbed 2D-IrB_{14} possess work functions of 5.10 and 4.8 eV, respectively, which are comparable with those for copper (~5.15 eV) and nickel (~4.92 eV) that are normally used as co-catalysts of photocatalysis reactions on TiO_2 or $SrTiO_3$.[43, 44] This indicates the potential of 2D-IrB_{14} for surface catalysis reactions.[45, 46] Upon the CO molecule adsorption on 2D-IrB_{14}, the work function is significantly reduced to 4.80 eV, which is measurable in experiment. Therefore, this might be another evidence that 2D-IrB_{14} can be a promising candidate for CO gas sensor materials.

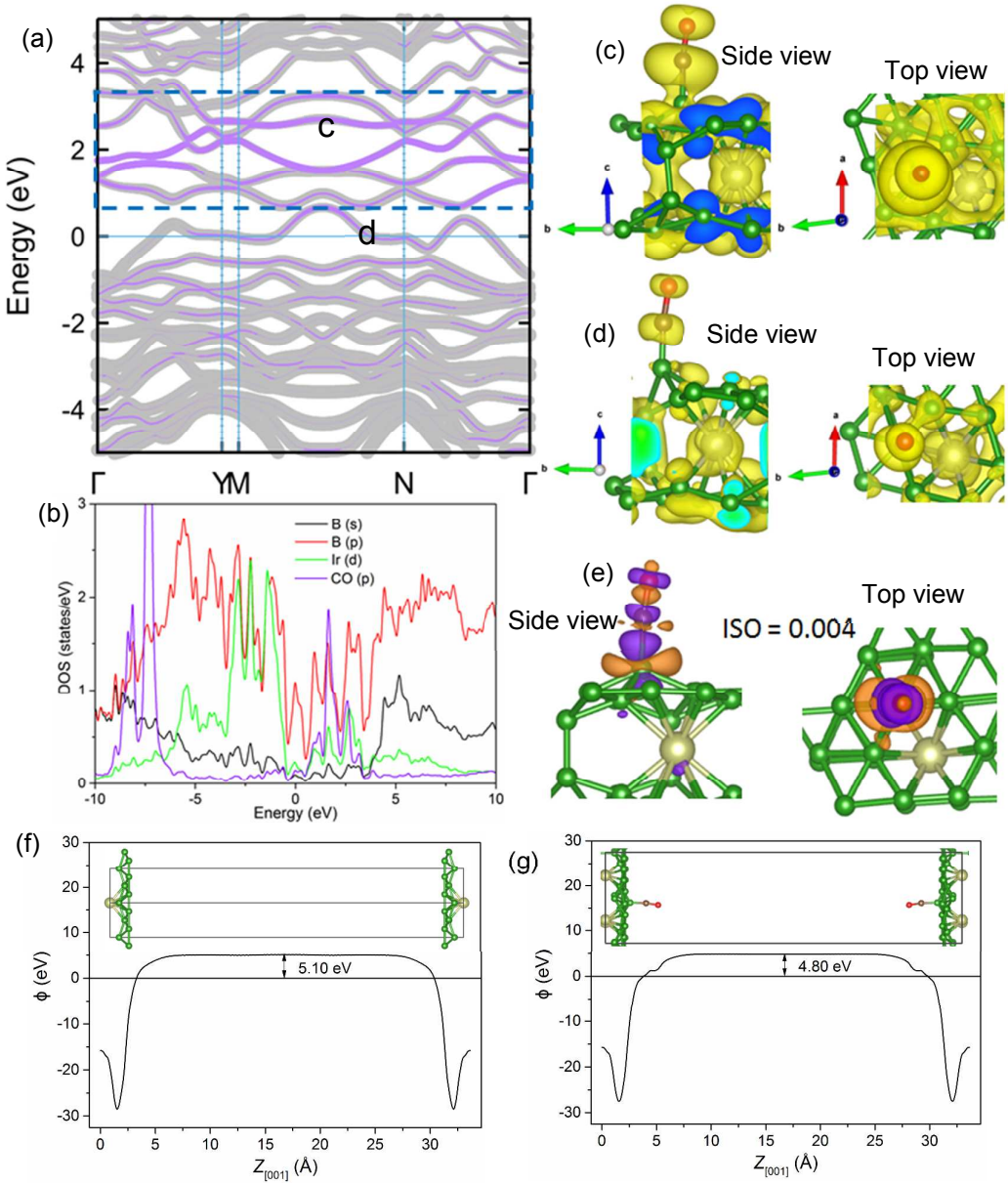

Figure 5 (a) Electronic band structure, (b) density of states (DOS), partial charge densities corresponding to the states (c) above and (d) across the Fermi energy, (e) charge density difference for the CO-adsorbed 2D-IrB_{14}, and the electrostatic (Hartree) potential as a function

of distance along [001] direction (perpendicular to the 2D surface) of pristine (f) and CO-adsorbed 2D-IrB_{14} (g). The interactions of CO molecule with B atom are highlighted in purple in the calculated electronic band structure.

Conclusions

Here, we predicted a series of stable sandwich-shaped structures for 2D iridium borides IrB_x through an ab initio evolutionary search. Among the predicated 2D systems, the most stable structure of 2D-IrB_{14} possesses an excellent thermodynamic stability with respect to the bulk Ir, stable 2D boron sheets, IrB_9 planar hypercodinate molecule and α-boron bulk. Phonon dispersion calculations as well as first-principles molecular dynamics (FPMD) simulations demonstrate its dynamic stability and confirm its thermal stability at elevated temperatures of up to 2000 K. Besides the much-improved stability, the electronic structure calculations show that in 2D-IrB_{14} the metallic feature of 2D boron sheet is kept after the introduction of iridium atoms. Moreover, we investigated the adsorption effects of the polluting CO and CO_2 molecules on the electronic structure of 2D-IrB_{14}. FPMD simulations and structure relaxations both show that on 2D-IrB_{14} the CO molecules are selectively adsorbed and form a strong bond with the surface. And the FPMD simulations reveal that the adsorbed CO molecules on 2D-IrB_{14} structure can be desorbed by simply heating to high temperature. Because of the significant charge transfer from 2D-IrB_{14} to the CO molecule, the electronic structure of CO/2D-IrB_{14} becomes different with that of the pristine one. Therefore, the present study suggests that 2D-IrB_{14} with synthesis possibility can be a promising candidate for gas sensing applications.

Conflicts of interest

There are no conflicts to declare.

Acknowledgements

The authors thank Prof. Artem R. Oganov of the Skolkovo Institute of Science and Technology for very useful advice. We acknowledge financial support from the Japan Society for the Promotion of Science (JSPS) through project P14207. This work was partly supported by the Core Research for Evolutional Science and Technology (CREST) program, Materials Research by Information Integration Initiative (MI2I) project of the Japan Science and Technology Agency (JST), Grant-in-Aid for Scientific Research of Japan Society for the Promotion of Science (JSPS) (Grant Numbers JP16K06713 and JP17H03234), and the World Premier International Research Center Initiative on Materials Nanoarchitectonics (MANA), MEXT.

References

1 A. R. Oganov, J. H. Chen, C. Gatti, Y. Z. Ma, Y. M. Ma, C. W. Glass, Z. X. Liu, T. Yu, O. O. Kurakevych, V. L. Solozhenko, Ionic high-Pressure Form of Elemental Boron, *Nature,* 2009, **457**, 863-867.

2 H. Tang, S. Ismail-Beigi, Novel Precursors for Boron Nanotubes: The Competition of Two-Center and Three-Center Bonding in Boron Sheets, *Phys. Rev. Lett.*, 2007, **99** 115501.

3 X. Wu, J. Dai, Y. Zhao, Z. Zhuo, J. Yang, X. C. Zeng, Two-Dimensional Boron Monolayer Sheets, *ACS Nano,* 2012, **6**, 7443-7453.

4 Y. Liu, E. S. Penev, B. I. Yakobson, Probing the Synthesis of Two-Dimensional Boron by First-Principles Computations, *Angew. Chem. Int. Ed.*, 2013, **52**, 3156-3159.

5 X. F. Zhou, X. Dong, A. R. Oganov, Q. Zhu, Y. J. Tian, H. T. Wang, Semimetallic Two-Dimensional Boron Allotrope with Massless Dirac Fermions, *Phys. Rev. Lett.*, 2014, **112**, 085502.

6 E. S. Penev, S. Bhowmick, A. Sadrzadeh, B. I. Yakobson, Polymorphism of Two-Dimensional Boron *Nano Lett.,* 2012, **12**, 2441-2445.

7 Z. Zhang, Y. Yang, G. Gao, B. I. Yakobson, Two-Dimensional Boron Monolayers Mediated by Metal Substrates, *Angew. Chem. Int. Ed.*, 2015, **54**, 13022-13026.

8 E. S. Penev, A. Kutana, B. I Yakobson. Can Two-Dimensional Boron Superconduct? *Nano Lett.*, 2016, **16**, 2522-2526.

9 X. F. Zhou, A. R. Oganov, Z. Wang, I. A. Popov, A. I. Boldyrev, H. T. Wang, Two-Dimensional Magnetic Boron, *Phys. Rev. B*, 2016, **93**, 085406

10 F. Ma, Y. Jiao, G. Gao, Y. Gu, A. Bilic, Z. Chen, A. Du, Graphene-like Two-Dimensional Ionic Boron with Double Dirac Cones at Ambient Condition, *Nano Lett.,* 2016, **16**, 3022-3028.

11 Z. Zhang, E. S. Penev, B. I. Yakobson, Polyphony in B flat, *Nat. Chem.,* 2016, **8**, 525-527.

12 Z. Zhang, A. J. Mannix, Z. Hu, B. Kiraly, N. P. Guisinger, M. C. Hersam, B. I. Yakobson, Substrate-Induced Nanoscale Undulations of Borophene on Silver, *Nano Lett.,* 2016, **16** 6622-6627.

13 A. J. Mannix, X. F. Zhou, B. Kiraly, J. D. Wood, D. Alducin, B. D. Myers, X. Liu, B. L. Fisher, U. Santiago, J. R. Guest, M. J. Yacaman, A. Ponce, A. R. Oganov, M. C. Hersam, N. P. Guisinger, Synthesis of Borophenes: Anisotropic Two-Dimensional Boron Polymorphs, *Science,* 2015, **350**, 1513-1516.

14 B. Feng, J. Zhang, Q. Zhong, W. Li, S. Li, H. Li, P. Cheng, S. Meng, L. Chen, K. Wu, Experimental Realization of Two-Dimensional Boron Sheets, *Nat. Chem.* 2016, **8**, 563-568.

15 G. Tai, T. Hu, Y. Zhou, X. Wang, J. Kong, T. Zeng, Y. You, Q. Wang, Synthesis of Atomically Thin Boron Films on Copper Foils, *Angew. Chem. Int. Ed.*, 2015, **54**, 15473-15477.

16 H. Zhang, Y. Li, J. Hou, K. Tu, Z. J. Chen, FeB_6 Monolayers: The Graphene-like Material with Hypercoordinate Transition Metal, *J. Am. Chem. Soc.* 2016, **138**, 5644-5651.

17 Y. Wang, J. Lv, L. Zhu, Y. Ma, Crystal structure prediction via particle-swarm optimization, *Phys. Rev. B,* 2010, **82**, 094116.

18 S. Xu, Y. Zhao, X. Yang, H. Xu, Stable sandwich structures of two-Dimensional Iron Borides FeBx alloy: A First-Principles Calculations, *RSC Adv.,* 2017, **7**, 30320.

19 A. R. Oganov, C. W. Glass, Crystal Structure Prediction using Ab Initio Evolutionary Techniques: Principles and Applications, *J. Chem. Phys.,* 2006, **124**, 244704.

20 C. W. Glass, A. R. Oganov, N. Hansen, USPEX-Evolutionary Crystal Structure Prediction. *Comput. Phys. Commun.,* 2006, **175**, 713-720.

21 Q. Zhu, L. Li, A. R. Oganov, P. B. Allen, Evolutionary Method for Predicting Surface Reconstructions with Variable Stoichiometry, *Phys. Rev. B*, 2013, **87**, 195317.

22 J. Wang, M. Khazaei, M. Arai, N. Umezawa, T. Tada, H. Hosono, Semimetallic Two-Dimensional TiB_{12}: Improved

Stability and Electronic Properties Tunable by Biaxial Strain, *Chem. Mater.,* 2017, **29**, 5922-5930.
23 C. Romanescu, T. R. Galeev, A. P. Sergeeva, W.-L. Li, L.-S. Wang, A. I. Boldyrev, Experimental and computational evidence of octa- and nona-coordinated planar iron-doped boron clusters: Fe©B8− and Fe©B9− *J, Organomet. Chem.,* 2012, 721-722, 148-154.
24 C. Romanescu, T. R. Galeev, W.-L. Li, A. I. Boldyrev, L.-S. Wang, Aromatic metal-centered monocyclic boron rings: Co©B8- and Ru©B9-, *Angew. Chem.* Int. Ed., 2011, **50**, 9334-9337.
25 W.-L. Li, C. Romanescu, T. R. Galeev, Z. A. Piazza, A. I. Boldyrev, L.-S. Wang, Transition-Metal-Centered Nine-Membered Boron Rings: M©B9 and M©B9-(M=Rh, Ir), *J. Am. Chem. Soc.,* 2012, **134**, 165-168.
26 J.V. Rau, A. Latini, New Hard and Superhard Materials: $RhB_{1.1}$ and $IrB_{1.35}$, *Chem. Mater.*, 2009, **21** (8), 1407–1409.
27 A. Latini, J. V. Rau, R. Teghil, A. Generosi, V. R. Albertini, ACS Appl. Mater. Interfaces, Superhard Properties of Rhodium and Iridium Boride Films, *ACS Appl. Mater. Interfaces*, 2010, **2** (2), 581–587.
28 G. Kresse, J. Furthmüller, Efficient Iterative Schemes for ab initio Total-Energy Calculations Using a Plane-Wave Basis Set, *Phys. Rev. B*, 1996, **54**, 11169.
29 G. Kresse, J. Furthmüller, Efficiency of ab-initio Total Energy Calculations for Metals and Semiconductors Using a Plane-Wave Basis Set, *Comput. Mater. Sci.*, 1996, **6**, 15-50.
30 J. Wang, N. Umezawa, H. Hosono, Mixed Valence Tin Ox-ides as Novel van der Waals Materials: Theoretical Predictions and Potential Applications, *Adv. Energy Mater.,* 2016, **6**, 1501190.
31 J. Wang, D. Hao, J. Ye, N. Umezawa, Determination of Crystal Structure of Graphitic Carbon Nitride: Ab Initio Evolutionary Search and Experimental Validation, *Chem. Mater.,* 2017, **29**, 2694-2707.
32 J.P. Perdew, A. Ruzsinszky, G.I. Csonka, O.A. Vydrov, G.E. Scuseria, L.A. Constantin, X. Zhou, and K. Burke, Restoring the Density-Gradient Expansion for Exchange in Solids and Surfaces, *Phys. Rev. Lett*. 2008, **100**, 136406.
33 S. Baroni, S. de Gironcoli, A. dal Corso, P. Giannozzi, Phonons and related crystal properties from density-functional perturbation theory, *Rev. Mod. Phys.,* 2001, **73**, 515-562.
34 S. J. Clark, M. D. Segall, C. J. Pickard, P. J. Hasnip, M. I. J. Probert, K. Refson, M. C. Payne, First principles methods using CASTEP, *Z. Kristallogr,* 2005, **220**, 567.
35 D. Karhánek, Self-Assembled Monolayers Studied by Density-Functional Theory, PhD Thesis, 2010.
36 F. Schedin, A. K. Geim, S. V. Morozov, E. W. Hill, P. Blake, M. I. Katsnelson, K. S. Novoselov, Detection of individual gas molecules adsorbed on grapheme, *Nat. Mater.,* 2007, **6**, 652.
37 J. Kong, N. Franklin, C. Zhou, M. Chapline, S. Peng, K. Cho, H. Dai, Nanotube Molecular Wires as Chemical Sensors, *Science,* 2000, **87**, 622.
38 P. G. Collins, K. Bradley, M. Ishigami, A. Zettl, Extreme oxygen sensitivity of electronic properties of carbon nanotubes, *Science,* 2000, **287**, 1801.
39 Y. Fujimoto, S. Saito, Gas adsorption energetics and electronic properties of boron- and nitrogen-doped bilayer graphenes, *Chemical Physics,* 2016, **478**, 55-61.
40 X. Liu, T. Ma, N. Pinna, J. Zhang, Two-Dimensional Nanostructured Materials for Gas Sensing, *Adv. Funct. Mater.* 2017, **27**, 1702168.
41 X. Wang, H. Qin, Y. Chen, J. Hu, Sensing Mechanism of SnO_2 (110) Surface to CO: Density Functional Theory Calculations, *J. Phys. Chem. C*, 2014, **118** (49), 28548–28561.
42 P. G. Lustemberg, D. A. Scherlis, Monoxide carbon frequency shift as a tool for the characterization of TiO_2 surfaces: Insights from first principles spectroscopy, *J. Chem. Phys.* 2013, **138**, 124702.
43 S. Paria, O. Reiser, Copper in Photocatalysis, *ChemCatChem,* 2014, **6**, 2477-2483.
44 A. W. Peters, Z. Li, O. K. Farha, J. T. Hupp, Toward Inexpensive Photocatalytic Hydrogen Evolution: A Nickel Sulfide Catalyst Supported on a High-Stability Metal-Organic Framework, *ACS Appl. Mater. Interfaces,* 2016, **8**, 20675-20681.
45 J. Park, T. Jin, C. Liu, G. Li, M. Yan, Three-Dimensional Graphene-TiO2 Nanocomposite Photocatalyst Synthesized by Covalent Attachment, *ACS Omega,* 2016, **1 (3)**, 351-356.
46 H. He, J. Lin, W. Fu, X. Wang, H. Wang, Q. Zeng, Q. Gu, Y. Li, C. Yan, B. K. Tay, C. Xue, X. Hu, S. T. Pantelides, W. Zhou, Z. Liu, MoS_2/TiO_2 Edge-On Heterostructure for Efficient Photocatalytic Hydrogen Evolution, *Adv. Energy Mater.,* 2016, **6**, 1600464.

TOC